

## Article

# An Optimized Design of the Soft Bellow Actuator Based on the Box–Behnken Response Surface Design

Jutamanee Auysakul <sup>1,\*</sup>, Apidet Booranawong <sup>2</sup>, Nitipan Vittayaphadung <sup>1</sup> and Pruittikorn Smithmaitrie <sup>1</sup>

<sup>1</sup> Department of Mechanical and Mechatronics Engineering, Faculty of Engineering, Prince of Songkla University, Songkhla 90110, Thailand; nitipan.v@psu.ac.th (N.V.); pruittikorn.s@psu.ac.th (P.S.)

<sup>2</sup> Department of Electrical Engineering, Faculty of Engineering, Prince of Songkla University, Songkhla 90110, Thailand; apidet.b@psu.ac.th

\* Correspondence: jutamanee.a@psu.ac.th

**Abstract:** Soft actuator technology is extensively utilized in robotic manipulation applications. However, several existing designs of soft actuators suffer from drawbacks such as a complex casting process, a multi-air chamber configuration, and insufficient grasping force. In this study, we propose a novel soft bellow design featuring a single air chamber, which simplifies the fabrication process of the actual model. To enhance the performance of the proposed design, we employ the Box–Behnken response surface design to generate a design matrix for implementing different levels of design factors in the finite element model. The FEA response is then subjected to an analysis of variance to identify significant factors and establish a regression model for deformation and stress response prediction. Among the considered responses, the wall thickness emerges as the most influential factor, followed by the divided ratio of radians and the number of bellows. Validation of the optimized soft bellow actuator’s deformation response is performed through comparison with experimental data. Moreover, the soft bellow actuator is capable of exerting a pulling force of 8.16 N when used in conjunction with a simple gripper structure design, enabling effective object manipulation. Additionally, the soft bellow design boasts cost-effectiveness and easy moldability, facilitating seamless integration with different gripper frames for diverse applications. Its simplicity and versatility make it a promising choice for various robotic manipulation tasks.

**Keywords:** soft bellow actuator; soft gripper; FEA; response surface analysis; Box–Behnken design



**Citation:** Auysakul, J.; Booranawong, A.; Vittayaphadung, N.; Smithmaitrie, P. An Optimized Design of the Soft Bellow Actuator Based on the Box–Behnken Response Surface Design. *Actuators* **2023**, *12*, 300. <https://doi.org/10.3390/act12070300>

Academic Editor: Hamed Rahimi Nohooji

Received: 11 June 2023

Revised: 16 July 2023

Accepted: 22 July 2023

Published: 24 July 2023



**Copyright:** © 2023 by the authors. Licensee MDPI, Basel, Switzerland. This article is an open access article distributed under the terms and conditions of the Creative Commons Attribution (CC BY) license (<https://creativecommons.org/licenses/by/4.0/>).

## 1. Introduction

In the automation industry, robot manipulation plays a pivotal role in process lines. The end-effector of a robot arm is a crucial component responsible for manipulating target objects through grasping [1]. Traditional grippers are designed with a rigid structure to handle specific items. However, they are unsuitable for gripping delicate or deformable objects encountered in manufacturing, such as food and fruit products, which lack stable geometry and possess complex surface properties. To overcome this limitation, soft grippers have been developed, offering the advantage of securely grasping objects with uneven shapes and precise positioning without causing damage [2]. This type of actuator has significantly enhanced the interaction between robots and object surfaces, prioritizing safety. Its applications extend beyond industrial work [3–5] and encompass fields like rehabilitation [6–9] and harvesting [10–12].

Soft grippers utilize various types of actuators [13] to hold, handle, and grasp objects, including pneumatic, vacuum, shape memory alloy, and cable-driven actuators. Among these, pneumatic actuators are highlighted in this study due to their adaptability and rapid response [14]. Soft pneumatic actuators exhibit a range of designs suitable for gripper applications [15]. One common design is pneumatic networks (PenuNets) [16–19], which involve the creation of multi-air chambers that utilize the bending effect to grip objects.

However, the fabrication process of the real model using silicone parts can be complicated, requiring the gluing together of multiple parts. Additionally, this design tends to provide a lower lift force when holding objects. To address these challenges, a more easily fabricated design called the fiber-reinforced design [20–22] has been proposed. This design features a single-celled air chamber covered with silicone and winding fiber, utilizing a bending state to hold objects. Another design approach, known as granular jamming [23], employs a donut-shaped structure with two chambers controlled by air pressure and vacuum to enclose objects, enabling the gripping of various sizes and shapes. Gao et al. [24] introduced a telescopic design with passive retraction and a gripping force of 14 N. On the other hand, the pneumatic bellow actuator [25–27] relies on rapid deformation responses achieved through compression and friction forces to grip objects. This design allows for direct control of deformation by adjusting the air pressure and is simpler to cast as a single chamber component. However, it provides limited information regarding optimal factors influencing deformation and stress response. To address these limitations, this research proposes an optimized design for the soft bellow actuator.

Response surface methodology (RSM) is a commonly used design of experiments (DOE) approach to determine the optimal influential factors in a given problem [28,29]. By employing statistical and mathematical techniques along with analysis of variance (ANOVA), this method facilitates the optimization and prediction of responses based on a set of independent variables. The approximating function is typically divided into first- and second-order models. Several design methodologies, such as the 3K factorial, central composite, and Box–Behnken designs, are commonly employed for second-order models [30]. The main advantage of the Box–Behnken design is its efficiency in exploring the design space and determining the optimal factor settings with a relatively small number of experiments. Compared to full factorial designs, the Box–Behnken design requires fewer experimental runs while still providing accurate and reliable results. This is particularly beneficial when conducting experiments that involve time-consuming or expensive simulations or physical prototypes.

In the context of soft actuator applications, Cao et al. [26] introduced the Box–Behnken design to optimize the parameters of a double-chamber bellow actuator, validating the displacement response through experimental data. Honarpardaz M. [31] utilized the Latin Hypercube Sampling Design with a full quadratic model to optimize the design of PenuNets, focusing on minimizing stress while maximizing the gripper’s payload. Chen et al. [32] utilized the topology optimization procedure to maximize the bending ability and enhance the payload capacity of the gripper. Finite element analysis (FEA) is a commonly employed technique to derive the response of an optimized design [33,34]. It serves as a valuable tool for enhancing the simulation model prior to manufacturing, saving time and eliminating the need for trial-and-error iterations.

This study aims to optimize the independent variables of the soft bellow actuator by employing a DOE approach with Box–Behnken response surface design. The objective is to achieve high deformation while minimizing stress. FEA is utilized to investigate the behavior of the soft bellow actuator in more than twenty cases. The proposed bellow design offers advantages in terms of fabrication process reduction by featuring a single air chamber and generating a significant pulling force that can be adapted for various applications. The framework presented in this work provides a systematic approach for researchers to optimize the soft actuator by reducing the design lead time and facilitating its application to other soft actuator models. The key objectives of this research can be summarized as follows:

- To study the parameters that influence the deformation response of the soft bellow actuator;
- To determine the optimized model of the soft bellow actuator and analyze the significant parameters using ANOVA;
- To propose a regression model to predict the deformation and stress response for this specific design of the soft bellow actuator;

- To validate the optimized design through experimental testing, assessing the deformation response and grasping performance using pulling force testing.

By addressing these objectives, this study provides valuable insights into the optimization of soft bellow actuators, enabling their efficient and effective use in various applications. The remainder of the article is organized as follows: Section 2 provides an overview of the workflow, the mathematical model of hyper-elastic materials, and the concept of DOE. Section 3 describes the geometric model of the soft bellow actuator and simulation analysis. Section 4 discusses significant parameters, the regression model, and the optimized design based on the Box–Behnken response surface design. Section 5 focuses on the manufacturing process and assembly of the soft bellow actuator. Section 6 presents the validation of the optimized design through deformation response and pulling-force performance. Finally, Section 7 concludes the paper, summarizing the findings and contributions of this study.

## 2. Materials and Methods

### 2.1. Workflow

The systematic workflow employed in this study is shown in Figure 1, which outlines the methodologies utilized. To assess the effectiveness of the optimized soft bellow actuator design, FEA is employed to identify the factors influencing deformation. These identified parameters are then applied to the Box–Behnken experimental design, generating a three-level design matrix. FEA is conducted using the MSC Marc Mentat Software (2020.0.0) to compute deformation and stress within the soft bellow actuator, allowing for the estimation of response parameters based on the generated design matrix. ANOVA is subsequently performed on the FEA results, calculating  $p$ -values to identify significant factors and establishing a regression model that correlates these factors with response parameters. By considering large deformation response and acceptable stress levels at a pneumatic pressure of 50 kPa, the optimal trial model within the design matrix is determined. To validate the deformation response of the optimized design, simulations are conducted and compared with experimental data. Subsequently, the soft bellow design is integrated into a rigid gripper structure to facilitate testing of its pulling force capabilities. By considering a large deformation response and acceptable stress levels at a pneumatic pressure of 50 kPa, the optimal trial model within the design matrix is determined. To validate the deformation response of the optimized design, simulations are conducted and compared with experimental data. Subsequently, the soft bellow design is integrated into a rigid gripper structure to facilitate testing of its pulling-force capabilities.

### 2.2. A Mathematical Model of Hyper-Elastic Materials

The soft bellow actuator incorporates a hyperelastic material for prototyping purposes, as it possesses the ability to undergo significant deformations when subjected to pressure, allowing for delicate object grasping [35]. In order to accurately characterize the hyperelastic behavior, nonlinear finite elements are employed. Various studies have proposed hyperelastic material models such as Mooney–Rivlin, Yeoh, Neo-Hookean, and Ogden by fitting experimental data curves. The numerical accuracy of these models relies on their order; however, a higher order does not necessarily guarantee a stronger correlation. For fundamental experiments like the uniaxial test, the two- or three-order Mooney–Rivlin approximation is commonly used [36]. The Mooney–Rivlin constitutive model is based on the strain energy function ( $W$ ). In the absence of volumetric deformation and temperature variations, this function can be expressed in polynomial form using MSC Marc Mentat Software (2020.0.0) as

$$W = \sum_{i+j=1}^n C_{ij}(I_1 - 3)^i (I_2 - 3)^j \quad (1)$$

where  $I_1$  and  $I_2$  are the deformation invariants, whereas  $C_{ij}$  are material-specific constants. These deformation invariants can be expressed as follows:

$$I_1 = \lambda_1^2 + \lambda_2^2 + \lambda_3^2 \tag{2}$$

$$I_2 = \lambda_1^2\lambda_2^2 + \lambda_2^2\lambda_3^2 + \lambda_3^2\lambda_1^2 \tag{3}$$

where  $\lambda_1$ ,  $\lambda_2$ , and  $\lambda_3$  are the elongations of the element in three directions, respectively.

The hyper-elastic material can be assumed to be incompressible by:

$$\lambda_1^2\lambda_2^2\lambda_3^2 = 1 \tag{4}$$

The elongation in each direction is a function of strain ( $\epsilon$ ), which can be presented by

$$\lambda = 1 + \epsilon \tag{5}$$

Thus, the deformation invariants for the uniaxial deformation mode can be expressed as follows:

$$I_1 = \lambda^2 + 2\lambda^{-1} \tag{6}$$

$$I_2 = 2\lambda + \lambda^{-2} \tag{7}$$

According to the Mooney–Rivlin three-order model, the stress ( $\sigma$ ) of the hyperelastic material can be defined in terms of elongation and the  $C_{ij}$  parameter as follows:

$$\sigma(\lambda) = 2[C_{10}(\lambda - \lambda^{-2}) + C_{01}(1 - \lambda^{-3}) + 3C_{11}(\lambda^2 - \lambda - 1 + \lambda^{-2} + \lambda^{-3} - \lambda^{-4})] \tag{8}$$

It is important to note that the internal pneumatic pressure can influence the elongation behavior of a flexible bellow actuator. The level of air pressure plays a significant role in determining the deformation and stress response of the actuator.

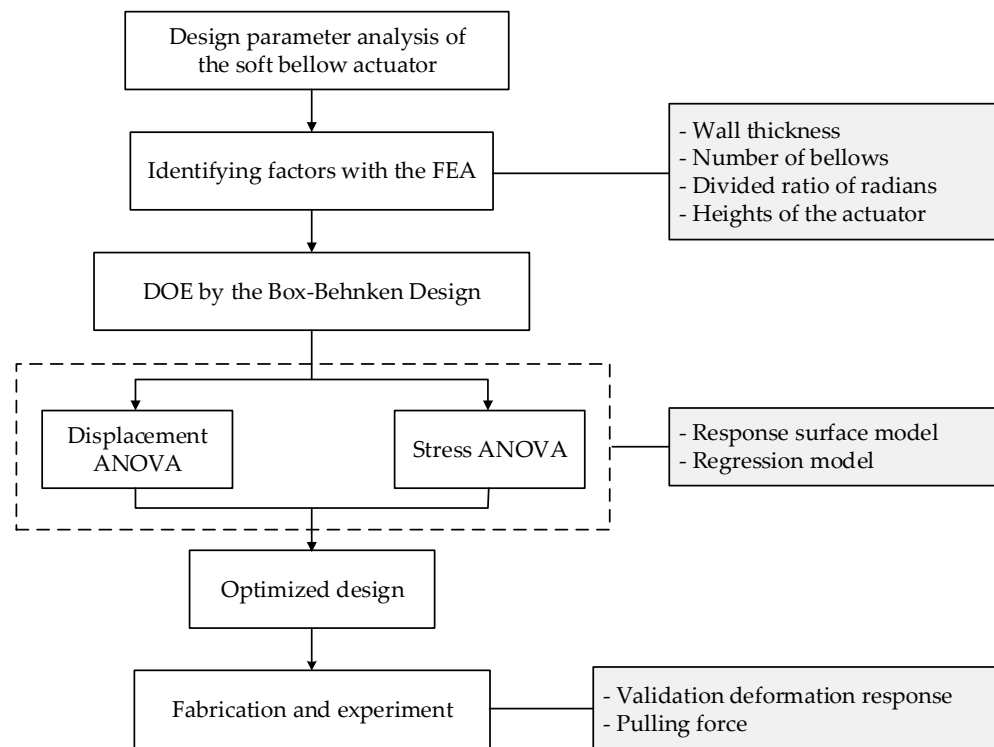


Figure 1. Analysis method.

### 2.3. Design and Statistical Analysis of Experiments

The Box–Behnken design is a well-known experimental design method that incorporates a response surface and is particularly suitable for investigating three independent variables in an experiment. Each factor is assigned code values representing the minimum, median, and maximum levels, resulting in three levels for each factor. These coded values facilitate the development of response surface designs. Additionally, to analyze the effect of parameters and estimate the regression equation, the Box–Behnken design response is employed. By considering the number of factors ( $K$ ) and the number of center points ( $P$ ), the total number of experiments ( $N$ ) can be determined using the following equation:

$$N = K^2 + K + P \quad (9)$$

The Box–Behnken response surface is generalized to the second order of the polynomial regression mode [30] as follows:

$$Y = \beta_0 + \sum_{i=1}^k \beta_i x_i + \sum_{i=1}^k \beta_{ii} x_i^2 + \sum_{i=1}^{k-1} \sum_{j=i+1}^k \beta_{ij} x_i x_j + \gamma \quad (10)$$

where  $Y$  is the response parameter;  $k$  is the number of independence variables ( $k = 3$ );  $x_i$  and  $x_j$  are the independence parameters;  $\beta_0$  is the intercept coefficient; and  $\beta_i$ ,  $\beta_{ii}$ , and  $\beta_{ij}$  are the regression coefficients for linear, quadratic, and interaction variables, respectively. The experimental miscalculation ( $\gamma$ ) is assumed to be zero. This regression model was used to estimate the factor responses. The fitness of the polynomial regression is defined by the coefficient of determination ( $R^2$ ). The significance of the factors is evaluated using ANOVA, employing the  $f$ -value at a specified  $p$ -value threshold. The optimal conditions for each factor are estimated through three-dimensional (3D) response surface plots and contour plots. Subsequently, the optimized model of the soft bellow actuator was validated by conducting experiments to verify the response.

## 3. Finite Element Analysis of Soft Bellow Design

### 3.1. Geometric Model of the Soft Bellow Actuator

The proposed design of the bellow actuator is shown in Figure 2. In this design, certain dimensions remain constant: the diameter on the top surface ( $D_1$ ) is 40 mm, the height of the soft actuator ( $H_1$ ) is 35 mm, and the length from the fixed base ( $H_2$ ) is 5 mm. The height of the bellows layer ( $h$ ) is determined by the number of bellows ( $N$ ) and the wall thickness ( $t$ ). The relationship between these parameters can be expressed as follows:

$$h = \frac{H_1 - H_2 - t}{N} \quad (11)$$

where  $h$  is used to compute the bellows' radius ( $r$ ) using the following formula:

$$r = \frac{h}{d} \quad (12)$$

where  $d$  is the divided ratio of  $h$  that must be more than half of  $h$  in order to calculate the  $r$  of the soft bellow actuator. In order to facilitate general usage for object grasping and to simplify the optimization process, the contact surface of the model is designed to be flat.

### 3.2. Simulation Analysis

FEA is a widely used tool for predicting the behavior of a system, including deformation, stress, and more. In this study, MSC Marc Mentat Software (2020.0.0) is utilized to perform FEA simulations. To reduce computational costs, an axisymmetric approach is employed to calculate the effects of deformation and stress. The model utilizes quadrilateral mesh elements with four nodes, as depicted in Figure 3.

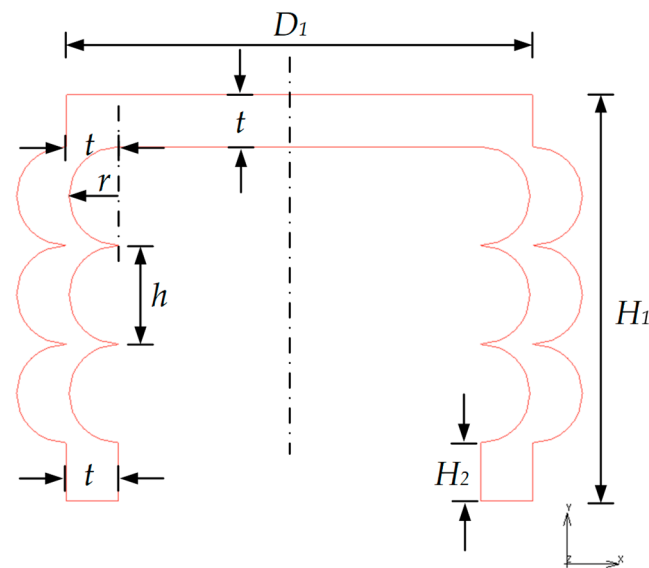


**Figure 2.** The geometry of the bellow design.

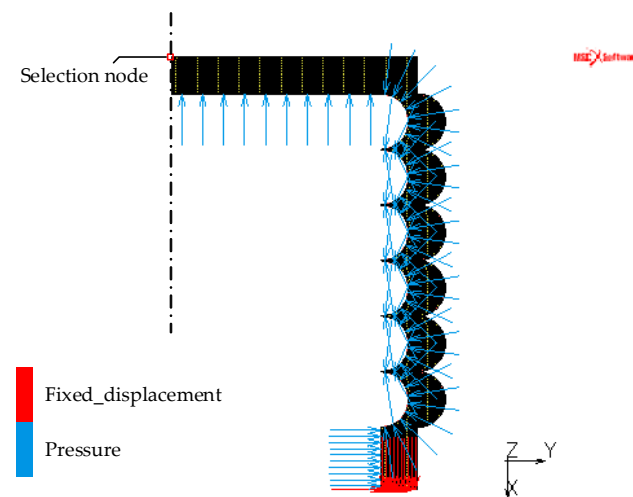


**Figure 3.** Boundary condition of an actuator.

Figure 3 shows the boundary conditions of the actuator with an axisymmetric model. In the analyzed model, the element type employs the full integration (Quad 10) formulation for solid structures. Given that the soft gripper deforms the actuator through pressurized air, several assumptions are made: (a) both the air pressure and atmospheric pressure are constant; (b) the actuator is completely sealed without any leaks; and (c) the pressure within the bellow is uniformly distributed and remains constant at each point. These assumptions allow for the definition of boundary conditions in the model. The ground of the actuator is subjected to a fixed displacement, while the inner surface of the curve generates pressure through an edge load, as illustrated in Figure 3. In this study, the edge load is set at 50 kPa, and a linear ramp table is employed to calculate the large strain of the static model with a constant time of 0.02, utilizing 50 steps. For model optimization, the deformation and stress response at the selected node, as shown in Figure 3, are considered. This particular location is crucial as it represents the weakest area responsible for supporting the object during grasping applications.

When it comes to applications involving soft actuators, materials like Ecoflex, Dragon Skin, and TPE rubber are commonly used for casting models. In this study, Dragon Skin 30 (Smooth-On, Inc., Macungie, PA, USA) was chosen as the material to construct the bellow actuator due to its desirable characteristics, including high tensile strength and significant

elongation deformation, which make it well-suited for gripper applications. The material properties of Dragon Skin 30 were evaluated for tensile strength using the ASTM D412 standard, employing a Z005 tensile testing machine (Zwick Roell, Ulm, Germany). Five silicone samples of Die C, each with a thickness of 3 mm, were subjected to extension at a rate of 500 mm/min until rupture. Figure 4 presents a comparison between the experimental data and the fitted data for the stress and strain of Dragon Skin 30. The maximum tensile strength was determined to be  $3.64 \pm 0.21$  MPa, while the elongation at break was measured to be  $473 \pm 28\%$ .

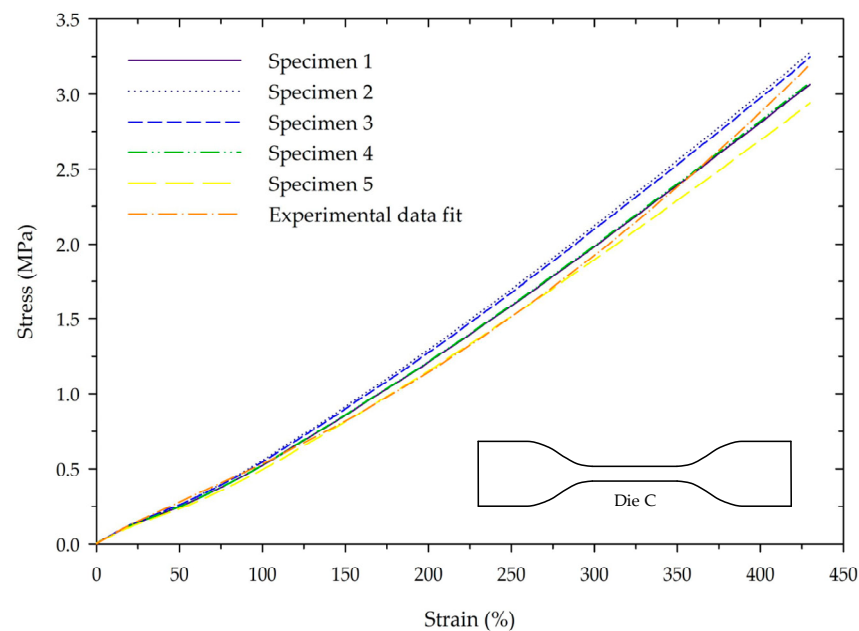


**Figure 4.** The tensile strength test data and experiment data fit.

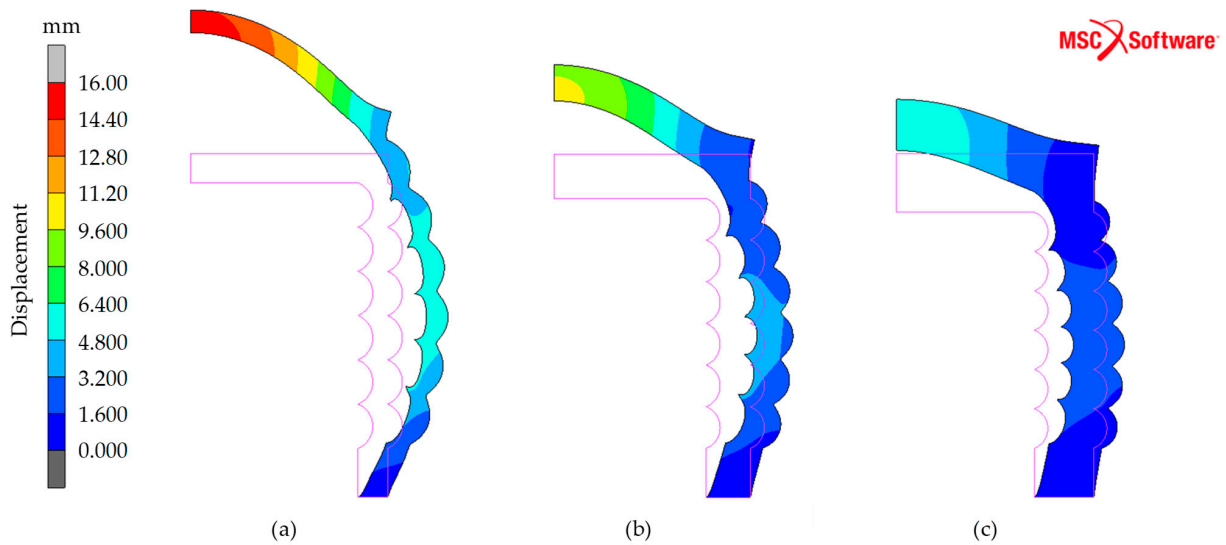
To determine the material properties, data from specimen 1 was selected for its average characteristics compared to the other specimens. The material properties were computed using MSC Marc Mentat software (2020.0.0). The Mooney–Rivlin model of the third order was utilized, with the following coefficients:  $C_{10} = 1.192 \times 10^{-1}$  MPa,  $C_{01} = 3.464 \times 10^{-9}$  MPa, and  $C_{11} = 1.484 \times 10^{-2}$  MPa, with an error  $3.370 \times 10^{-4}$ . To optimize the design of the soft bellow gripper, the deformation and stress at the center of the model's upper surface were analyzed. These response parameters were crucial for the DOE using the Box–Behnken method, allowing for the design of the bellow soft gripper with acceptable levels of deformation and stress.

In this study, we consider the following factors to influence the deformation of the soft bellow actuator: wall thickness, number of bellows, bellow radian, and actuator height. These factors are crucial in defining the response prior to applying the Box–Behnken method for factor reduction. The wall thickness is examined at three levels: 3 mm, 4.5 mm, and 6 mm. The casting process imposes a minimum wall thickness requirement, as thin walls are prone to tearing.

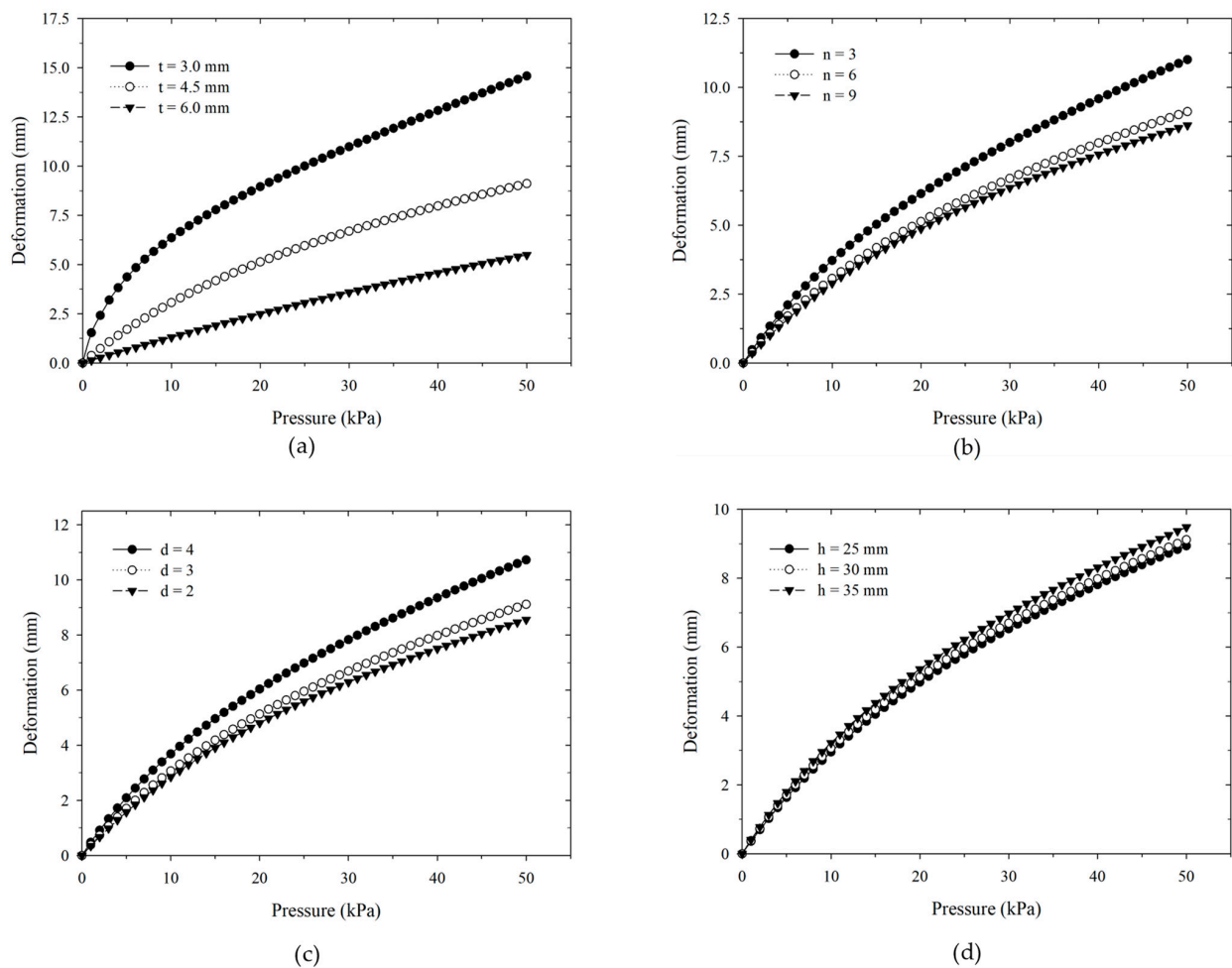
The simulation models in our study maintain a consistent number of bellows (six) and a divided ratio for the bellow radian (three). Figure 5 demonstrates the finite element analysis result of the comparative model. The lower part of the model, represented by the blue color, indicates fixed displacement, while the middle portion of the model's upper surface, depicted in red, exhibits significant displacement. This region is influenced by the internal pressure of the actuator and is located away from the fixing area.

Figure 6a presents the relationship between deformation displacement and pressure for comparable wall thicknesses. At a pressure of 50 kPa, the 3 mm wall thickness demonstrates the highest deformation displacement of 14.58 mm, whereas the 6 mm wall thickness exhibits the smallest deformation displacement of 5.49 mm. It is evident that the thin wall

thickness significantly affects the deformation of the soft actuator. However, it is important to note that excessive stress on a thin wall may lead to actuator rupture.



**Figure 5.** Simulation result of deformation response under 50 kPa pressure with different wall thicknesses of (a) 3 mm, (b) 4.5 mm, and (c) 6 mm.



**Figure 6.** Relationship between deformation and air pressure of simulation results (a) under different wall thicknesses, (b) under different numbers of bellows, (c) under different divided ratios, and (d) under different heights of the actuator.

We compare the deformation response for three different numbers of bellows: three, six, and nine, simulated under the same conditions, as previously described. The models for comparison have the same wall thickness and a divided ratio of 4.5 mm and 3, respectively. In Figure 6b, it can be observed that the deformation with varying numbers of bellows at six and nine under the same pressure is not dissimilar. When the applied pressure is 50 kPa, the greatest deformation displacement of 11.0 mm is observed with three bellows. The deformation responses of these three cases are comparable, as the rigidity of the simulation model does not vary significantly.

Next, we examine the effect of the bellow's radian with different divided ratios of two, three, and four while keeping the same wall thickness (4.5 mm) and number of bellows (six). Figure 6c demonstrates the influence of the bellow's radian on the deformation response. The divided ratio of four yields the greatest deformation of 10.72 mm compared to the divided ratios of two and three. However, most of the models exhibit deformations greater than 8 mm, which is beneficial when adapting the model to a soft actuator for a wide range of object grasping.

Furthermore, when comparing the height of the actuator at 25 mm, 30 mm, and 35 mm with the same wall thickness (4.5 mm), number of bellows (six), and divided ratio of radians (three), Figure 6d illustrates that the actuator's height has no significant effect on the deformation response. The nearly identical deformations observed in each air-pressurized simulation case confirm that the actuator's height does not significantly influence the deformation response. Hence, the factors that have a notable impact on the deformation of the actuator include the wall thickness, number of bellows, and divided ratio of radians. These variables were used to create an experiment using the Box–Behnken method, allowing for the optimization of the model.

#### 4. Box–Behnken Design

The optimization of the soft bellow actuator's design focuses on the deformation and stress at the contact surface. To achieve this goal, the Box–Behnken technique is employed to optimize the model's design through a matrix design. This method utilizes a response surface to determine the effect of factors and levels on the objective function. In this study, the deformation of the soft gripper was influenced by the wall thickness, number of bellows, and divided ratio of radians, as described in Section 2.3. In the Box–Behnken design, these factors are used to evaluate the surface response, with the index *A* representing the wall thickness (mm), *B* representing the number of bellows, and *C* representing the divided ratio of radians. The deformation and stress results at the selection node are denoted by *D* (mm) and *E* (kPa), respectively. Table 1 provides an overview of how the factors are classified into three levels.

**Table 1.** Design factors of the Box–Behnken method.

Factor	Name	Low	Median	High
<i>A</i>	Wall thickness	3	4.5	6
<i>B</i>	Number of bellows	3	6	9
<i>C</i>	Divided ratio of radians	2	3	4

The response surface design of the soft bellows is investigated using three factors and three levels. Equation (9) is used to calculate the total number of experiments, and the replicate number is three. As a result, the simulation test employs the design factors based on the Box–Behnken design, as shown in Table 2. The number of trials is equal to the number of experiments, totaling 15 cases. This parameter is utilized to define an optimum soft bellow design with high deformation and minimal stress.

**Table 2.** Box–Behnken design and response results.

Standard Order	Running Order	Point Type	Blocks	A	B	C	D	E
1	1	2	1	3	3	3	18.06	290.8
2	2	2	1	6	3	3	6.49	243.9
3	3	2	1	3	9	3	13.28	287.9
4	4	2	1	6	9	3	5.19	234.1
5	5	2	1	3	6	2	19.02	288.2
6	6	2	1	6	6	2	6.37	250.1
7	7	2	1	3	6	4	13.19	289.7
8	8	2	1	6	6	4	5.14	232.0
9	9	2	1	4.5	3	2	16.07	294.6
10	10	2	1	4.5	9	2	9.52	294.3
11	11	2	1	4.5	3	4	9.50	288.6
12	12	2	1	4.5	9	4	8.27	290.8
13	13	0	1	4.5	6	3	9.12	291.8
14	14	0	1	4.5	6	3	9.12	291.8
15	15	0	1	4.5	6	3	9.12	291.8

### Analysis of Variance

The response surface with the Box–Behnken design is utilized to determine the influence of the deformation and stress of the bellow actuator, as observed from the FEA results presented in Table 2. The displacement response is subjected to ANOVA at a 95% confidence level, and the results are summarized in Table 3. The model  $f$ -value of 273.89 and the associated  $p$ -value ( $p < 0.0001$ ) indicate that the regression model is statistically significant. The mean square (MS) value for the uncontrolled aspect of the simulation data had an inaccuracy of 0.1127. The analysis of the model's significant factors suggests that the  $p$ -values should be less than 0.05, with variables having lower  $p$ -values being more significant.

**Table 3.** Results of the ANOVA for extraction displacement of the soft bellow actuator.

Source	DF	Adj SS	Adj MS	F-Value	$p$ -Value
Model	9	277.84	30.87	273.89	<0.0001
Linear					
A	1	203.59	203.59	1806.27	<0.0001
B	1	23.97	23.97	212.64	<0.0001
C	1	27.68	27.68	245.6	<0.0001
Square					
A×B	1	2.76	2.76	24.49	0.0043
B×C	1	2.22	2.22	19.66	0.0068
C×C	1	3.31	3.31	29.38	0.0029
2-way Interaction					
A×B	1	3.05	3.05	27.02	0.0035
A×C	1	5.3	5.3	47.01	0.001
B×C	1	7.06	7.06	62.65	0.0005
Error	5	0.5636	0.1127		
Total	14	278.4			

$R^2 = 0.998$ ,  $\text{adj-}R^2 = 0.9943$ ,  $\text{C.V.}\% = 3.2$ , and  $\text{Adeq Precision} = 51.55$

As seen in Table 3, all variables, including linear, quadratic, and two-way interactions, have  $p$ -values less than 0.05, indicating their significant influence on the displacement response. The Adeq Precision is a measure of signal-to-noise ratio precision, with values greater than four indicating high precision. In this case, the Adeq Precision is 51.55, suggesting that the design space navigation model had a high level of precision. Through

the analysis of displacement simulation data using multiple regression, the response model in the second-order polynomial equation can be predicted using Equation (13):

$$D = 76.26 - 10.287A - 3.811B - 13.65C + 0.3843A \times A + 0.0861B \times B + 0.947C \times C + 0.1939A \times B + 0.767A \times C + 0.4429B \times C \quad (13)$$

The  $R^2$  and  $\text{adj-}R^2$  values for this regression model are 0.998 and 0.9943, respectively. These values exceed 0.7, indicating a significant correlation between the displacement response and the independent variables.  $R^2$  values closer to 1 suggest that the regression model is well-suited to the actual response.

Figure 7 presents the 3D response surface and contour plot of the regression equation (Equation (13)). These plots provide insights into the relationship between the displacement response and the levels of two independent variables. The results of the extraction affected by the wall thickness, number of bellows, and divided ratio of radians are displayed in Figure 7a–c. Using two continuous variables and fixing the other variable at its middle, Figure 7a illustrates the displacement response as a function of wall thickness and number of bellows while keeping the radian ratio constant at three. These two factors had a significant impact on increasing the deformation of the bellow actuator. The response range increases rapidly from 9.12 to 18.06 mm when the wall thickness is reduced below 4.5 mm. In Figure 7b, the effect of the divided ratio of radians and the number of bellows is shown, with the wall thickness kept constant at 4.5 mm. The displacement response increases as the parameter values decrease.

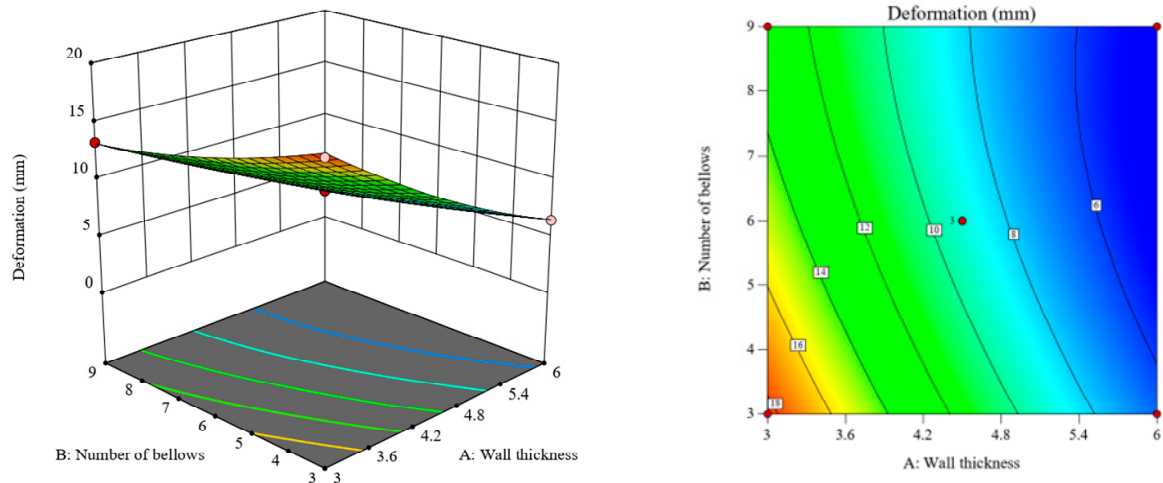
However, when the divided ratio of radians exceeds four, the displacement response of the model is restricted to a range of 13 mm. Figure 7c presents the response of the divided ratio of radians and the wall thickness, with the number of bellows kept constant at six. Reducing the values of these two factors leads to an increase in the deformation response within the range of 8.58 to 15.76 mm. Therefore, the regression model response highlights the significant influence of wall thickness on the displacement response, as the stiffness of the actuator depends on this factor. It is followed by the divided ratio of radians and the number of bellows.

Table 4 presents the ANOVA results based on the experimental stress data of the bellow actuator using the Box–Behnken design. The regression model exhibits a  $p$ -value close to zero and a high  $f$ -value of 119.83, indicating its overall effectiveness and significance. Factors  $A$ ,  $C$ ,  $A \times A$ , and  $A \times C$  have high significance for the stress response, as their  $p$ -values are less than 0.05, while other factors have negligible effects. The regression model for the stress response of the soft bellow actuator is expressed by Equation (14).

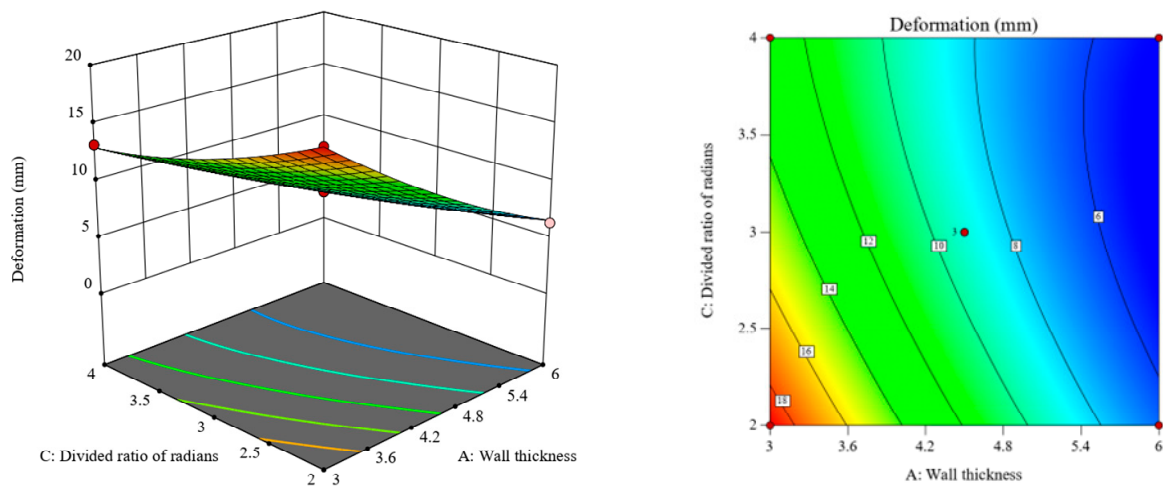
$$E = 85.2 + 105.06A + 0.94B + 6.92C - 12.146A \times A - 0.027B \times B + 0.55C \times C - 0.381A \times B - 3.280A \times C + 0.215B \times C \quad (14)$$

The regression model for stress prediction demonstrates a good fit to the experimental data, with  $R^2$  and  $\text{adj-}R^2$  values of 0.9954 and 0.9871, respectively. This indicates that the model accurately predicts the stress of the actuator.

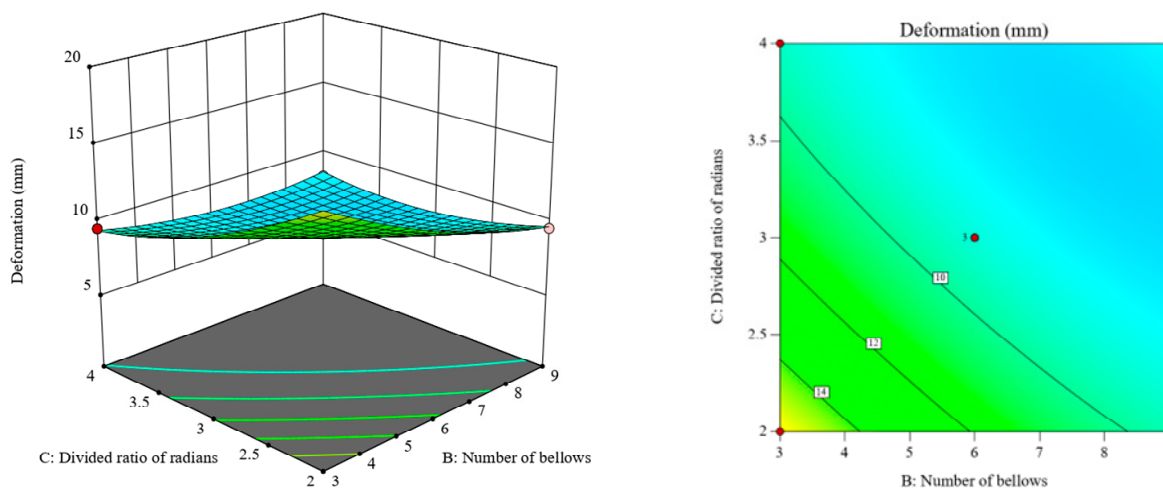
Figure 8 shows the response of the deformation and stress of the soft bellow actuator based on the trial numbers in the Box–Behnken design. The models with thick walls of 6 mm (trial numbers 2, 4, 6, and 8) exhibit a deformation response of less than 6.5 mm and a minimum stress in the range of 230–250 kPa. These models have high wall stiffness, resulting in lower deformation and stress. For the model with a wall thickness of 4.5 mm, trial numbers 10 to 15 show a deformation response of less than 10 mm, except for trial number 9. Trial number 9 has the minimum values for the number of bellows and the divided ratio of radians, leading to a higher deformation response. However, the stress response of all models with a 4.5 mm wall thickness is approximately 290 kPa.



(a)



(b)



(c)

**Figure 7.** Response surface and contour diagrams of the soft bellow: (a) under constant the divided ratio of radians, (b) under constant the number of bellows, and (c) under constant the wall thickness.

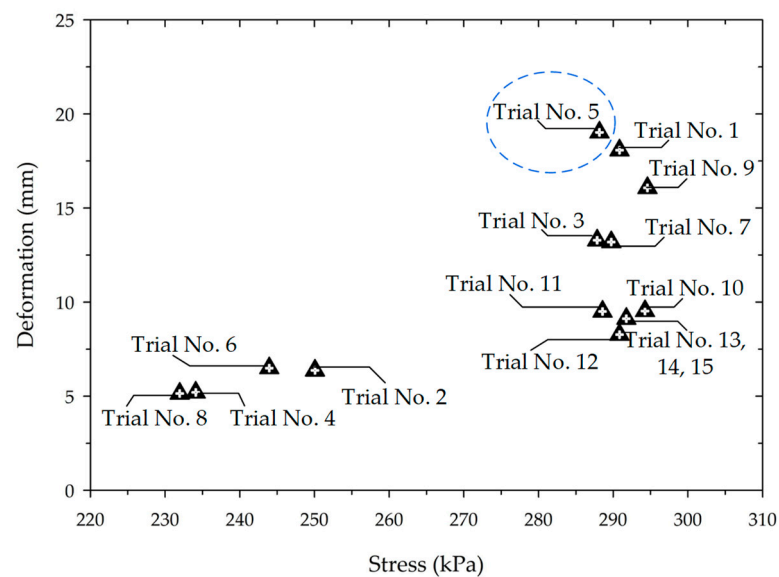


**Figure 8.** The Box–Behnken design matrix responds to stress and deformation.

**Table 4.** Results of the ANOVA for the extraction stress of the soft bellow actuator.

Source	DF	Adj SS	Adj MS	F-Value	<i>p</i> -Value
Model	9	7830.61	870.07	119.83	<0.0001
Linear					
A	1	4827.23	4827.23	664.82	<0.0001
B	1	14.86	14.86	2.05	0.212
C	1	84.18	84.18	11.59	0.0191
Square					
A×A	1	2757.63	2757.63	379.79	<0.0001
B×B	1	0.2251	0.2251	0.031	0.8671
C×C	1	1.12	1.12	0.1541	0.7108
2-way Interaction					
A×B	1	11.73	11.73	1.62	0.2597
A×C	1	96.82	96.82	13.33	0.0147
B×C	1	1.67	1.67	0.2299	0.6518
Error	5	36.3	7.26		
Total	14	7866.92			

$R^2 = 0.9954$  and  $\text{adj-}R^2 = 0.9871$ ,  $C.V.\% = 0.9716$ , and  $\text{Adeq Precision} = 29.572$

In contrast, the models with a thin wall thickness of 3 mm (trial numbers 1, 3, 5, and 7) exhibit a deformation response greater than 13 mm. Among these models, trial number 5, with the number of bellows and the ratio of radii is six and two, respectively. It demonstrates a significant amount of deformation. However, trial number 5 has a lower stress response compared to trial number 1 and 9, due to its greater rigidity. Therefore, trial number 5 represents the optimal design for the actuator, as it achieves high displacement while maintaining an appropriate stress level.

## 5. Manufacturing and Assembly

In this section, we proceeded to construct the physical model based on the optimized design from trial number 5 in the previous section. The optimized model has a wall thickness of 3 mm, six bellows, and a divided ratio of radii of two. The fabrication process of the soft bellow gripper involves two main components: the soft bellow part and the rigid frame structure. For the soft bellow part, a molding process is employed using

the hyper-elastic material. This design features a single air chamber, which simplifies the fabrication process. The trial number 5 model has a volume of  $16,567 \text{ mm}^3$  and weighs  $17.89 \text{ g}$ , considering the density of Dragon Skin 30 at  $1.08 \text{ g/cm}^3$ . Figure 9 shows the four steps involved in the casting process. The model's mold is divided into five pieces for easy disassembly and was created using a 3D printer, specifically the Flashforge Adventurer 3 (Zhejiang Flashforge 3D Technology Co., Ltd., Jinhua, China).

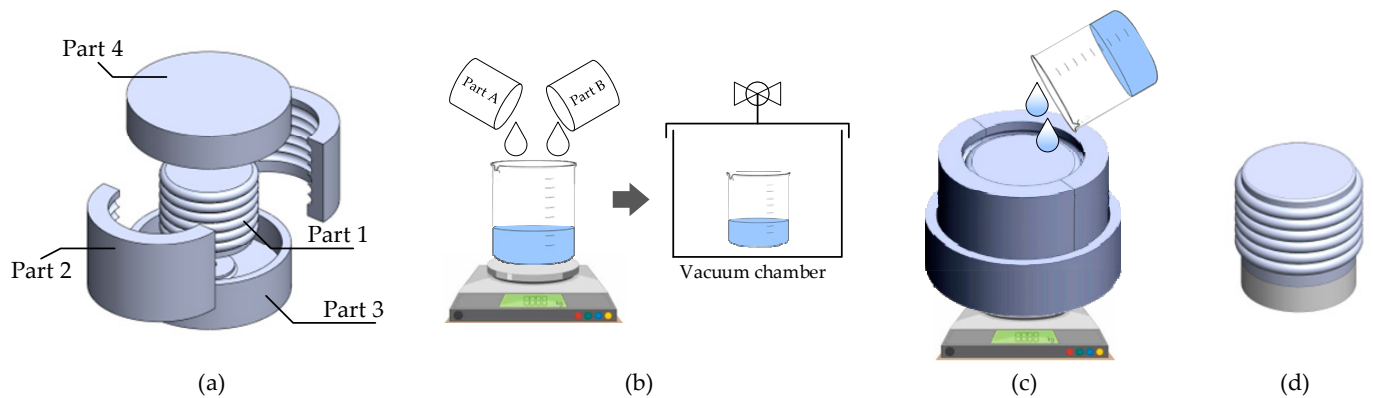


**Figure 9.** Fabrication of a Soft Bellow Actuator: (a) 3D-printed molds, (b) silicone preparation, (c) casting process, and (d) final assembly.

In the assembly steps, Part 1 of the mold is attached to Part 3 using a screw. To ensure proper fitting during mold construction, a tolerance of 10% is maintained between Part 2 and Part 3. Next, Dragon Skin 30, consisting of Part A and Part B in a 1:1 weight-to-weight ratio, is prepared. The silicone compound is thoroughly mixed, and any bubbles in the mixture are eliminated using a vacuum chamber. The liquid silicone is carefully poured into the mold, with the mass of the silicone being measured accurately. An additional 5% weight is added to account for any potential mold leakage. To ensure the optimal quality of the final product, the mold is shaken to eliminate any trapped air bubbles within the silicone. Once the pouring and shaking process is complete, the top surface of the mold is securely closed using Part 4. Subsequently, the silicone is left to cure for approximately 16 h at room temperature. Alternatively, it can be cured at a higher temperature to expedite the curing process.

The rigid frame of the gripper is specifically designed to enable the grasping and holding of objects, resembling the functionality of human fingers. For the purpose of this study, only two soft bellow actuators were utilized to evaluate the basic grasping properties of the optimized actuator. The frame structure, as depicted in Figure 10, consists of three individual components: the support plate for the soft bellow component, the gripping frame, and the holding plate. All of these parts were fabricated using 3D printing technology. The support plate serves the purpose of securely attaching the soft bellow component to the rigid part. Additionally, it includes a hose connector that supplies pressurized air to the soft actuator. To ensure a strong bond between the silicone part and the rigid part, an ethyl-based instant glue called Loctite 495, manufactured by Henkel AG & Co. KGaA, in Dusseldorf, Germany, is applied. The gripping frame is specifically designed to facilitate the grasping of objects with two fingers, accommodating objects ranging from 30 to 50 mm in size. It is connected to the holding plate, which serves the dual function of providing support for the end-effectors of the robot arm (Dobot CR5) during experimental procedures and enabling future applications such as pick-and-place operations.

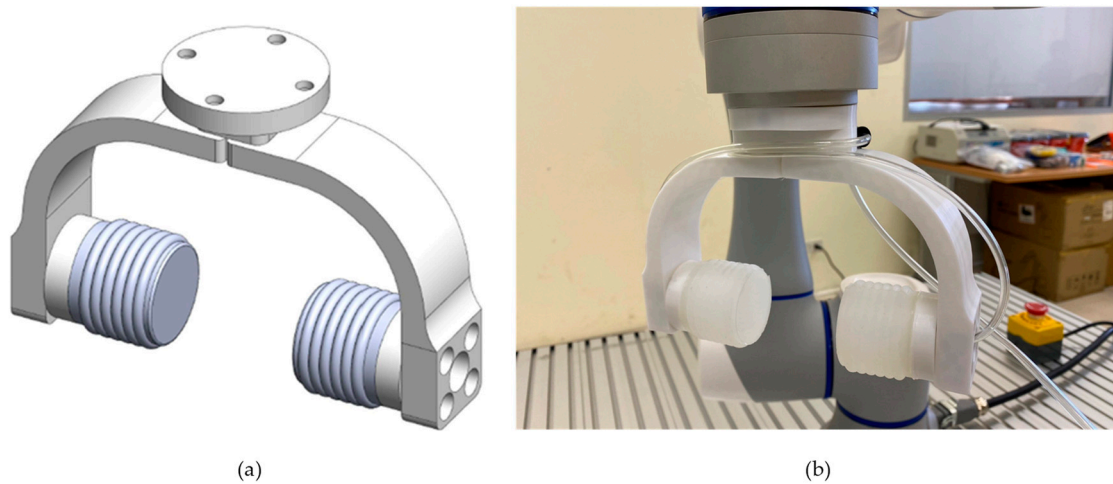


**Figure 10.** Assembly of the rigid frame and the soft bellow actuator (a) in the 3D model and (b) in the real model.

## 6. Experiments and Results

This study focused on evaluating the performance of the soft bellow actuators and the associated pulling force. To conduct these tests, the air pressure was carefully regulated using a digital regulator, specifically the SMC ITV2050 model. This regulator offers a pressure range of 0.005 to 0.9 MPa and has a quick response time of 0.1 s. To control the actuated air pressure, a voltage divider circuit was employed. This circuit allows for the adjustment of the output voltage within the range of 0 to 10 VDC using a potentiometer. By varying the output voltage, the desired air pressure for actuation can be achieved. The electrical and pneumatic systems are interconnected, as illustrated in Figure 11, providing a schematic representation of their setup and integration.

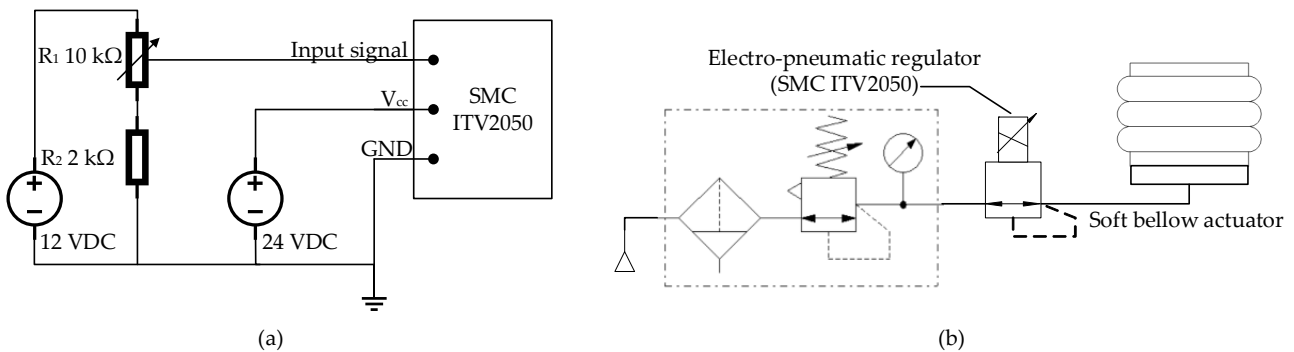


**Figure 11.** Schematic diagram of (a) the electrical system and (b) the pneumatic system.

### 6.1. Validation of the Deformation Response

The response of the soft bellow actuator to fluctuations in internal air pressure was evaluated to verify the accuracy of the optimized simulation model. The pneumatic pressure was adjusted in 5 kPa increments from 0 to 50 kPa. The displacement of the actuator was measured at steady internal air pressure conditions. This experiment was conducted five times with five samples to investigate the deformation response of the actuator. Figure 12 illustrates the deformation performance of the optimized soft bellow actuator at different internal air pressures. The actuator exhibited inflation as the pressure increased, with a maximum pressure limit of 50 kPa to prevent damage to the bellows.

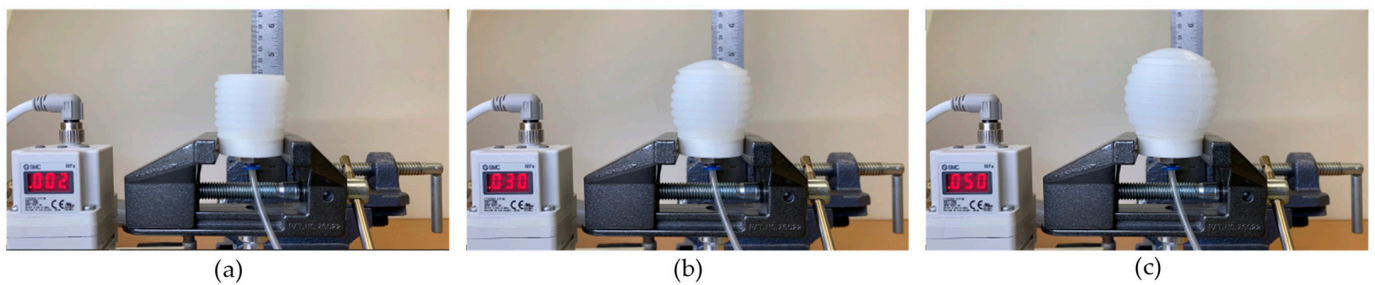


**Figure 12.** The deformation response at different air pressure levels: (a) at 2 kPa, (b) at 30 kPa, and (c) at 50 kPa.

Figure 13 shows a comparison of the deformation responses between the experimental and simulation results. In the pneumatic pressure range of 0 to 20 kPa, the experimental deformation showed a high error compared to the simulation, with an average error of 43.12%, or 3.22 mm. However, for pressures exceeding 25 kPa, the deformation of both the experiment and simulation results became more similar, with an error range of 2.51–2.18 mm or an average error of 14.54%. These discrepancies can be attributed to several factors, including material properties, manufacturing tolerances, boundary conditions, and simplified assumptions.

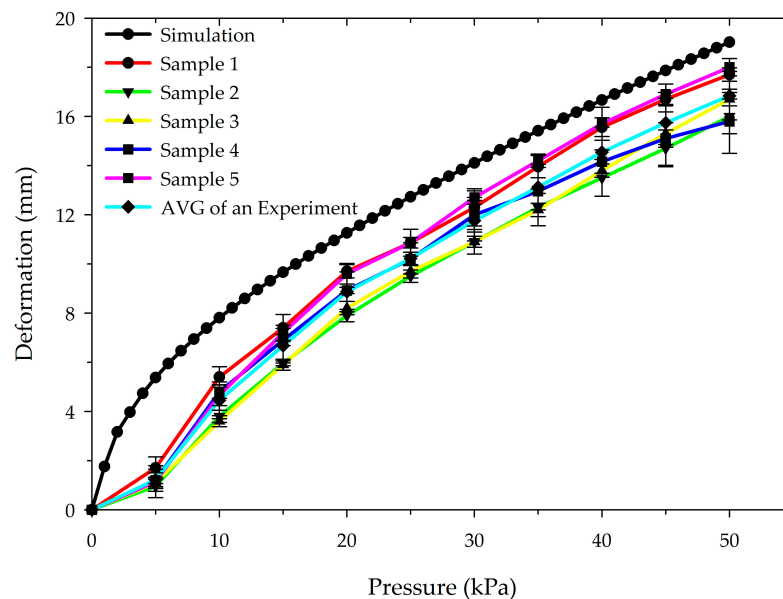


**Figure 13.** Comparison of deformation responses.

The material properties in the simulation, such as the elastic modulus and strain energy function of the soft bellow actuator of the Mooney–Rivlin model, may not accurately represent the actual properties, leading to differences between the predicted and experimental deformations. Additionally, the simulation assumes an idealized model without considering manufacturing imperfections, such as uneven thickness or slight variations in material properties, which can impact the behavior of the actuator and result in deviations from the experimental results. The boundary conditions in the simulation, which aim to replicate the experimental setup, may not precisely mimic the actual conditions, further contributing to differences in deformation. The simplified assumptions made in the simulation, particularly using an axisymmetric model, can also introduce inaccuracies, especially in scenarios involving intricate or nonlinear deformations at low pressures.

Furthermore, Table 5 provides a comparison of the deformation and strain between the experimental and simulation results. The experimental deformation reached 16.84 mm, while the analytical model was limited to 19.02 mm, resulting in a difference of less than

2.18 mm compared to the simulation. The strain values were 0.481% and 0.543% for the experiment and simulation, respectively, with an error of 11.46%. These variations can be attributed to the aforementioned factors influencing the inflation behavior of the soft bellow actuator, leading to the experimental response being lower than the simulation result. However, both the experimental and simulation results demonstrate a satisfactory deformation response.

**Table 5.** The deformation and strain of the optimized design.

Pressure (kPa)	Deformation (mm)		Strain (%)		% Error of a Deformation
	Experiment (Average)	Simulation	Experiment (Average)	Simulation	
5	1.22	5.37	0.035	0.153	−77.29
10	4.452	7.81	0.127	0.223	−42.99
15	6.672	9.66	0.191	0.276	−30.92
20	8.864	11.26	0.253	0.322	−21.29
25	10.224	12.73	0.292	0.364	−19.68
30	11.76	14.11	0.336	0.403	−16.63
35	13.124	15.41	0.375	0.440	−14.85
40	14.544	16.66	0.416	0.476	−12.72
45	15.74	17.86	0.450	0.510	−11.89
50	16.84	19.02	0.481	0.543	−11.46

### 6.2. Pulling force Experiment

The experimental setup for measuring the pulling force of the soft bellow gripper is depicted in Figure 14. The gripper, designed as per the proposed model, is mounted on a robot arm. Various objects, including a cube, a cylinder, and a sphere with a diameter of 50 mm, were grasped by the soft bellow gripper. To measure the pulling force, a digital force gauge (SF-100 Model, Wenzhou Sanhe Instrument Co., Ltd., Wenzhou, China) was attached to the tested object. The response of the gripper was evaluated at different levels of internal air pressure, ranging from 20 to 40 kPa.

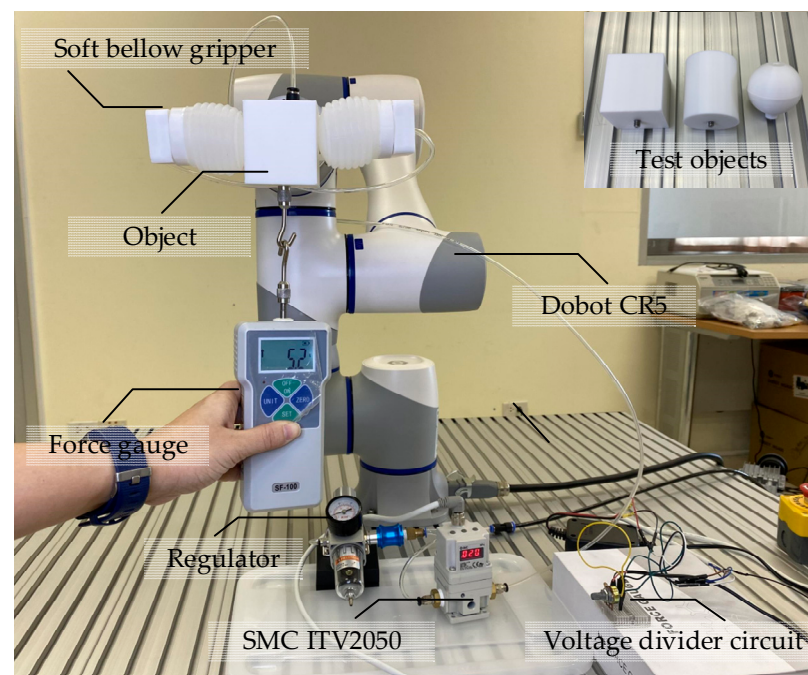


**Figure 14.** Experimental setup for pulling with different objects.

The response of the gripper was evaluated at different levels of internal air pressure, ranging from 20 to 40 kPa. Figure 15 presents the performance of the gripper in holding objects at different pressure levels. It can be observed that as the air pressure increased, the deformation of the actuator applied a compressive force to the object. However, excessive pneumatic pressure exceeding 40 kPa can adversely affect the contact force, potentially leading to actuator damage.

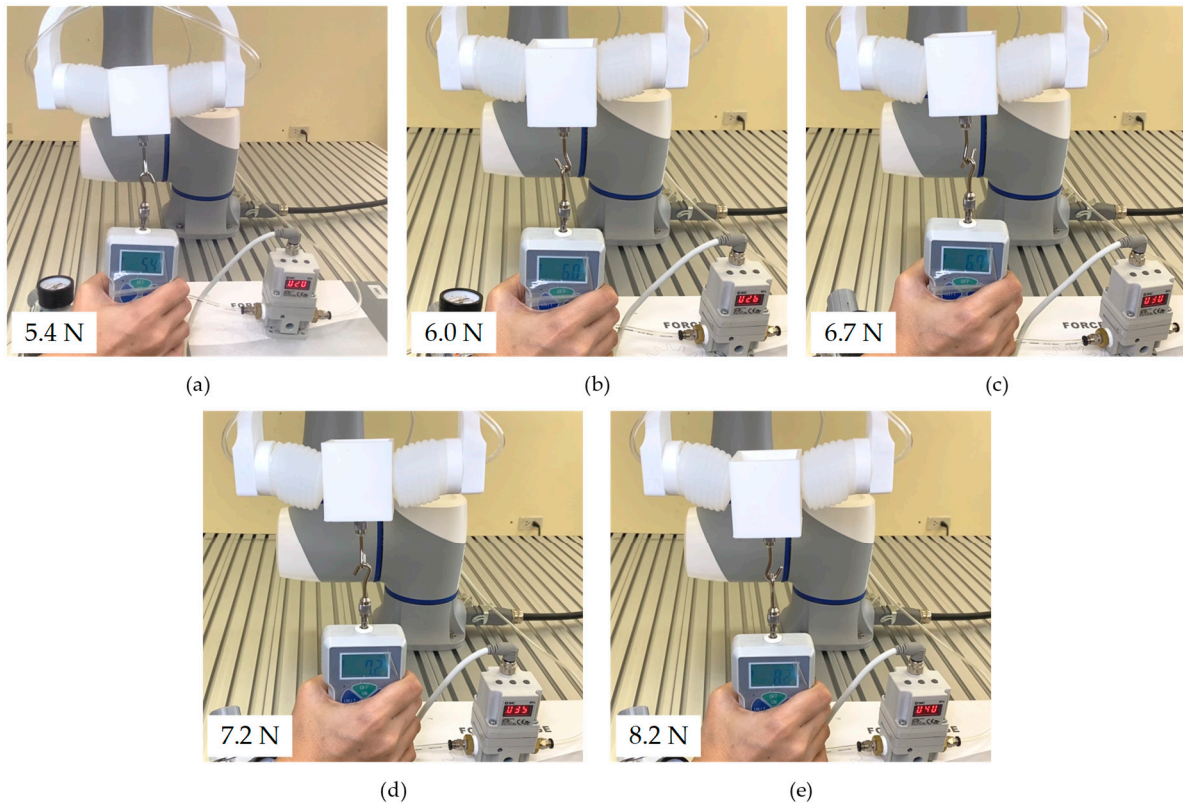


**Figure 15.** Responses of the pulled gripper at different air pressure levels of (a) 20 kPa, (b) 25 kPa, (c) 30 kPa, (d) 35 kPa, and (e) 40 kPa.

Figure 16 provides a comparison of the average pulling force exerted on different object shapes. The cube shape exhibited the highest gripping force ( $8.16 \pm 0.30$  N), followed by the cylindrical shape ( $7.14 \pm 0.80$  N) and the spherical shape ( $5.18 \pm 0.08$  N), all tested at 40 kPa. This difference in pulling force can be attributed to the variation in the contact surface area between the gripper and the objects. The cube shape offered a larger contact surface area, resulting in a stronger grip. The pulling force response to pressure changes was linear for each object shape, with the cube and cylinder objects exhibiting a higher rate of pulling force response compared to the sphere object. The designed and optimized soft bellow actuator demonstrated its capability to grasp various object shapes with a robust pulling force. Notably, the cost of the soft bellow prototype is remarkably low, amounting to only USD 1.22, while the total price of the robotic gripper is also economical at USD 5.90.

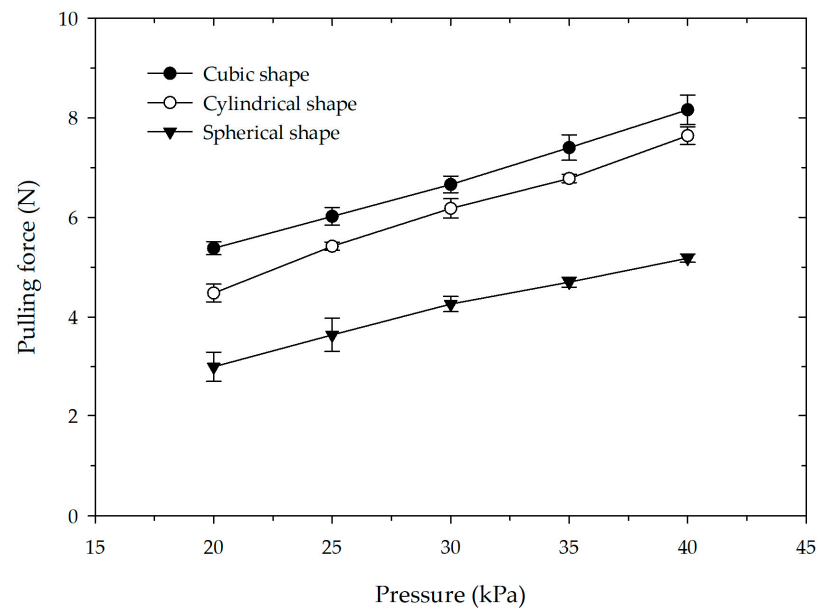


**Figure 16.** The result of pulling force on different shapes of objects.

## 7. Conclusions

This study aimed to optimize the design of the soft bellow actuator by considering factors such as wall thickness, number of bellows, and divided ratio of radians, as they significantly affect the deformation and stress response. To achieve this, we employed FEA and a Box–Behnken response surface design, resulting in a design matrix comprising 15 experimental models. Through variance analysis using ANOVA, we identified the key factors influencing the deformation and stress response, with wall thickness emerging as the most significant factor, followed by the divided ratio of radians and the number of bellows. Upon analyzing the design matrix, we determined Trial number 5 to be the optimized design for the soft bellow actuator. This design demonstrated substantial deformation and allowable stress when subjected to maximum air pressure. A comparison between the experimental and simulation results revealed a satisfactory deformation response, with an error rate of approximately 11.46% at high pressure, or 2.18 mm less than the optimized simulation model.

Additionally, we evaluated the pulling-force performance of the validated soft bellow actuator model by integrating two actuators into a rigid gripper structure. The experimental results demonstrated the capability of the soft bellow gripper to grasp objects of various shapes, achieving a maximum holding force of 8.16 N. Consequently, the optimized design and regression model of the soft bellow actuator can be employed in numerical models to assess the suitability of the soft gripper. Additionally, the fabrication process is simplified with the use of a single air chamber, and the displacement of the actuator can be easily controlled by adjusting the pneumatic pressure. Furthermore, the design of the soft bellow gripper offers the flexibility to be integrated with different rigid frames, enabling efficient object grasping in a wide range of applications. This design's versatility allows for its adaptation to various scenarios, thereby enhancing its potential for broader implementation.

**Author Contributions:** Conceptualization and methodology, J.A. and P.S.; formal analysis and investigation, J.A. and N.V.; writing—original draft preparation, J.A.; writing—review and editing, A.B. and P.S.; supervision, J.A. and P.S. All authors have read and agreed to the published version of the manuscript.

**Funding:** This work was supported by Research and Development Office, Prince of Songkla University, Thailand under Grant ENG6502013S.

**Data Availability Statement:** Not applicable.

**Conflicts of Interest:** The authors declare no conflict of interest.

## References

- Samadikhoshkho, Z.; Zareinia, K.; Janabi-Sharifi, F. A Brief Review on Robotic Grippers Classifications. In Proceedings of the 2019 IEEE Canadian Conference of Electrical and Computer Engineering (CCECE), Edmonton, AB, Canada, 5–8 May 2019; pp. 1–4.
- Li, M.; Pal, A.; Aghakhani, A.; Pena-Francesch, A.; Sitti, M. Soft Actuators for Real-World Applications. *Nat. Rev. Mater.* **2022**, *7*, 235–249. [[CrossRef](#)]
- Garcia Rubiales, F.J.; Ramon Soria, P.; Arrue, B.C.; Ollero, A. Soft-Tentacle Gripper for Pipe Crawling to Inspect Industrial Facilities Using Uavs. *Sensors* **2021**, *21*, 4142. [[CrossRef](#)] [[PubMed](#)]
- Morikage, O.; Wang, Z.; Hirai, S. Multi-Fingered Soft Gripper Driven by Bellows Actuator for Handling Food Materials. In Proceedings of the 2021 27th International Conference on Mechatronics and Machine Vision in Practice (M2VIP), Shanghai, China, 26–28 November 2021; pp. 363–368.
- Hu, Q.; Dong, E.; Sun, D. Soft Gripper Design Based on the Integration of Flat Dry Adhesive, Soft Actuator, and Microspine. *IEEE Trans. Robot.* **2021**, *37*, 1065–1080. [[CrossRef](#)]
- Pan, M.; Yuan, C.; Liang, X.; Dong, T.; Liu, T.; Zhang, J.; Zou, J.; Yang, H.; Bowen, C. Soft Actuators and Robotic Devices for Rehabilitation and Assistance. *Adv. Intell. Syst.* **2022**, *4*, 2100140. [[CrossRef](#)]
- Heung, H.L.; Tang, Z.Q.; Shi, X.Q.; Tong, K.Y.; Li, Z. Soft Rehabilitation Actuator with Integrated Post-Stroke Finger Spasticity Evaluation. *Front. Bioeng. Biotechnol.* **2020**, *8*, 111. [[CrossRef](#)]
- Sun, Z.; Guo, Z.; Tang, W. Design of Wearable Hand Rehabilitation Glove with Soft Hoop-Reinforced Pneumatic Actuator. *J. Cent. South Univ.* **2019**, *26*, 106–119. [[CrossRef](#)]
- Polygerinos, P.; Wang, Z.; Galloway, K.C.; Wood, R.J.; Walsh, C.J. Soft Robotic Glove for Combined Assistance and At-Home Rehabilitation. *Robot. Auton. Syst.* **2015**, *73*, 135–143. [[CrossRef](#)]
- Navas, E.; Fernández, R.; Armada, M.; Gonzalez-de-Santos, P. Diaphragm-Type Pneumatic-Driven Soft Grippers for Precision Harvesting. *Agronomy* **2021**, *11*, 1727. [[CrossRef](#)]
- Ranasinghe, H.N.; Kawshan, C.; Himaruwan, S.; Kulasekera, A.L.; Dassanayake, P. Soft Pneumatic Grippers for Reducing Fruit Damage During Strawberry Harvesting. In Proceedings of the 2022 Moratuwa Engineering Research Conference (MERCon), Moratuwa, Sri Lanka, 27–29 July 2022; pp. 1–6.
- Navas, E.; Dworak, V.; Weltzien, C.; Fernández, R.; Shokrian Zeini, M.; Käthner, J.; Shamshiri, R. An Approach to the Automation of Blueberry Harvesting Using Soft Robotics. *43. GIL-Jahrestag. Resiliente Agri-Food-Syst.* **2023**, pp. 435–440. Available online: <https://dl.gi.de/server/api/core/bitstreams/9cf3b7f2-150d-4c51-951e-b8b40390d9f3/content> (accessed on 10 June 2023).
- Zaidi, S.; Maselli, M.; Laschi, C.; Cianchetti, M. Actuation Technologies for Soft Robot Grippers and Manipulators: A Review. *Curr. Robot. Rep.* **2021**, *2*, 355–369. [[CrossRef](#)]
- Chen, R.; Zhang, C.; Sun, Y.; Yu, T.; Shen, X.-M.; Yuan, Z.-A.; Guo, J.-L. A Paper Fortune Teller-Inspired Reconfigurable Soft Pneumatic Gripper. *Smart Mater. Struct.* **2021**, *30*, 045002. [[CrossRef](#)]
- Walker, J.; Zidek, T.; Harbel, C.; Yoon, S.; Strickland, F.S.; Kumar, S.; Shin, M. Soft Robotics: A Review of Recent Developments of Pneumatic Soft Actuators. *Actuators* **2020**, *9*, 3. [[CrossRef](#)]
- Wang, Z.; Or, K.; Hirai, S. A Dual-Mode Soft Gripper for Food Packaging. *Robot. Auton. Syst.* **2020**, *125*, 103427. [[CrossRef](#)]
- Mosadegh, B.; Polygerinos, P.; Keplinger, C.; Wennstedt, S.; Shepherd, R.F.; Gupta, U.; Shim, J.; Bertoldi, K.; Walsh, C.J.; Whitesides, G.M. Pneumatic Networks for Soft Robotics That Actuate Rapidly. *Adv. Funct. Mater.* **2014**, *24*, 2163–2170. [[CrossRef](#)]
- Auysakul, J.; Vittayaphadung, N.; Gonsrang, S.; Smithmaitrie, P. Bending Angle Effect of The Cross-Section Ratio for a Soft Pneumatic Actuator. *Int. J. Mech. Eng. Robot. Res.* **2020**, *9*, 366–370. [[CrossRef](#)]
- Zhang, X.; Yu, S.; Dai, J.; Oseyemi, A.E.; Liu, L.; Du, N.; Lv, F. A Modular Soft Gripper with Combined Pneu-Net Actuators. *Actuators* **2023**, *12*, 172. [[CrossRef](#)]
- Cheng, P.; Ye, Y.; Yan, B.; Lu, Y.; Wu, C. Eccentric High-Force Soft Pneumatic Bending Actuator for Finger-Type Soft Grippers. *J. Mech. Robot.* **2022**, *14*, 060908. [[CrossRef](#)]
- Ye, Y.; Cheng, P.; Yan, B.; Lu, Y.; Wu, C. Design of a Novel Soft Pneumatic Gripper with Variable Gripping Size and Mode. *J. Intell. Robot Syst.* **2022**, *106*, 5. [[CrossRef](#)]
- Polygerinos, P.; Wang, Z.; Overvelde, J.T.; Galloway, K.C.; Wood, R.J.; Bertoldi, K.; Walsh, C.J. Modeling of Soft Fiber-Reinforced Bending Actuators. *IEEE Trans. Robot.* **2015**, *31*, 778–789. [[CrossRef](#)]
- Joseph, T.; Baldwin, S.; Guan, L.; Brett, J.; Howard, D. The Jamming Donut: A Free-Space Gripper Based on Granular Jamming. *arXiv* **2022**, arXiv:2212.06485.
- Gao, G.; Chang, C.M.; Gerez, L.; Liarokapis, M. A Pneumatically Driven, Disposable, Soft Robotic Gripper Equipped with Multi-Stage, Retractable, Telescopic Fingers. *IEEE Trans. Med. Robot. Bionics* **2021**, *3*, 573–582. [[CrossRef](#)]
- Guo, N.; Sun, Z.; Wang, X.; Yeung, E.H.K.; To, M.K.T.; Li, X.; Hu, Y. Simulation Analysis for Optimal Design of Pneumatic Bellow Actuators for Soft-Robotic Glove. *Biocybern. Biomed. Eng.* **2020**, *40*, 1359–1368. [[CrossRef](#)]
- Cao, M.; Zhu, J.; Fu, H.; Loic, H.Y.F. Response Surface Design of Bellows Parameters with Negative Pressure Shrinkage Performance. *Int. J. Interact. Des. Manuf. (IJIDeM)* **2022**, *16*, 1041–1052. [[CrossRef](#)]

27. Müller, D.; Sawodny, O. Modeling the Soft Bellows of the Bionic Soft Arm. *IFAC-PapersOnLine* **2022**, *55*, 229–234. [[CrossRef](#)]
28. Dean, A.; Voss, D.; Draguljić, D. Response Surface Methodology. In *Design and Analysis of Experiments*; Dean, A., Voss, D., Draguljić, D., Eds.; Texts in Statistics; Springer International Publishing: Cham, Switzerland, 2017; pp. 565–614. ISBN 978-3-319-52250-0.
29. Kleijnen, J.P.C. Response Surface Methodology. In *Handbook of Simulation Optimization*; Fu, M.C., Ed.; International Series in Operations Research & Management Science; Springer: New York, NY, USA, 2015; pp. 81–104. ISBN 978-1-4939-1384-8.
30. Khuri, A.I.; Mukhopadhyay, S. Response Surface Methodology. *WIREs Comput. Stat.* **2010**, *2*, 128–149. [[CrossRef](#)]
31. Honarpardaz, M. A Methodology for Design and Simulation of Soft Grippers. *Simulation* **2021**, *97*, 779–791. [[CrossRef](#)]
32. Chen, F.; Xu, W.; Zhang, H.; Wang, Y.; Cao, J.; Wang, M.Y.; Ren, H.; Zhu, J.; Zhang, Y.F. Topology Optimized Design, Fabrication, and Characterization of a Soft Cable-Driven Gripper. *IEEE Robot. Autom. Lett.* **2018**, *3*, 2463–2470. [[CrossRef](#)]
33. Tawk, C.; Alici, G. Finite Element Modeling in the Design Process of 3D Printed Pneumatic Soft Actuators and Sensors. *Robotics* **2020**, *9*, 52. [[CrossRef](#)]
34. Guo, L.; Li, K.; Cheng, G.; Zhang, Z.; Xu, C.; Ding, J. Design and Experiments of Pneumatic Soft Actuators. *Robotica* **2021**, *39*, 1806–1815. [[CrossRef](#)]
35. Marechal, L.; Baland, P.; Lindenroth, L.; Petrou, F.; Kontovounisios, C.; Bello, F. Toward a Common Framework and Database of Materials for Soft Robotics. *Soft Robot.* **2021**, *8*, 284–297. [[CrossRef](#)]
36. Szurgott, P.; Jarzębski, Ł. Selection of a Hyper-Elastic Material Model—a Case Study for a Polyurethane Component. *Lat. Am. J. Solids Struct.* **2019**, *16*, 1–16. [[CrossRef](#)]

**Disclaimer/Publisher’s Note:** The statements, opinions and data contained in all publications are solely those of the individual author(s) and contributor(s) and not of MDPI and/or the editor(s). MDPI and/or the editor(s) disclaim responsibility for any injury to people or property resulting from any ideas, methods, instructions or products referred to in the content.